The spatial and temporal characterization of type IV creep fracture in notched specimen of modified 9Cr-1Mo steel

Tsuruta, H.
IHI Corporation

Toda, H.
Kyushu University

Hirayama, K.
Kyushu University

Shimizu, K.
Kyushu University

他

出版情報：Materials Science and Engineering: A. 902, pp.146607-, 2024-06. Elsevier
バージョン：
権利関係：

The spatial and temporal characterization of type IV creep fracture in notched specimen of modified 9Cr-1Mo steel

H. Tsuruta[*1], H. Toda[*2], K. Hirayama[*2], K. Shimizu[*2], H. Fujihara[*2], A. Takeuchi[*3] and M. Uesugi[*3]

*1 IHI Corporation

*2 Kyushu University

*3 Japan Synchrotron Radiation Research Institute

In order to observe type IV fracture occurring in the HAZ fine-grained zone of a modified 9Cr-1Mo steel at high resolution, the creep damage process of a single notched specimen was continuously observed in three dimensions. The initiation, growth and coalescence behaviour of individual creep voids were clearly observed. This was combined with an analysis of the local stress state using the finite element method. Furthermore, all creep voids that could be observed in the final loading stage were traced backward in time to determine the loading stages at which the creep voids were initiated together with the growth behaviour of the individual creep voids. Significant creep void formation was observed a little further in from the bottom of the notch, where the maximum principal and hydrostatic stresses were greatest, while the stress triaxiality was greatest a little closer to the centre of the specimen than the maximum principal and hydrostatic stresses, where significant creep void growth was observed. It was found that the creep voids nucleated at an early loading stage dominated the creep failure of the specimen. The growth behaviour could be well approximated by the model that combined the diffusion law and power creep law with the constraint effect from neighbouring grains. Engineering parameters that describe the progress of type IV damage were also investigated.

Keywords: Modified 9Cr-1Mo steel, Fine-grained HAZ, Creep void, 4D observation, X-ray micro-tomography, Damage initiation and growth, Creep model.

1. Introduction.

Creep rupture of structural metallic materials is important from the perspective of ensuring the long-term reliability of various components used in high-temperature environments. Although it is difficult to prevent creep rupture completely, it is possible to delay its occurrence and propagation by controlling microstructure. Microstructural changes occur at high temperatures, such as microstructural coarsening, phase changes and changes in chemical composition. It is therefore important to improve the thermal stability of the metallurgical microstructure [1-3]. On the other hand, focusing on the creep rupture process, creep rupture consists of the formation, growth and coalescence of creep voids and the subsequent formation and propagation of macroscopic cracks [4]. Of these, the initial creep void formation, growth and coalescence processes are particularly closely related to the microstructure of the material [5, 6] and are important in terms of creating materials with high creep fracture resistance. However, unlike macroscopic crack behaviour that can be observed from the surface, microscopic void formation inside materials is difficult to evaluate quantitatively. This is partly because the voids disappear during cutting and polishing in conventional cross-sectional evaluations. Moreover, even if the voids are completely preserved during cutting and polishing, two-dimensional observation does not allow the true shape, size and clustering of voids and their 3D spatial distribution to be determined [7, 8 "Section 8.5, Quantitative Geometric Analysis, pp. 476 – pp. 481"].

Among the creep failures of steel, Type IV failure, which occurs in highly alloyed precipitation-strengthened steels such as 9 % Cr steels, is well known [9-11]. This is creep fracture caused by the formation of creep voids in the heat-affected zone (hereinafter HAZ) of welded joints and is a fracture phenomenon that has not yet been overcome in industries such as the power industry. The mechanism of Type IV fracture is due to the coarsening of precipitates in the HAZ by over-aging [12,13]. The presence of the resulting creep-softened zone localises the deformation to a narrow HAZ bands formed along the melt pool, leading to damage [14]. However, damage does not occur uniformly within the HAZ.

Thus, it is extremely difficult to accurately identify and evaluate creep ruptures that occur locally in specific areas. This requires an unconventional approach using a state-of-the-art scientific equipment: X-ray microtomography, which has been used in earnest in science and engineering since the 21st century, is the most suitable technique for studying material damage because it allows non-destructive, three-dimensional characterisation. High-resolution 3D images of microscopic defects caused by casting, various forming processes and heat treatment, as well as deformation, damage and fracture during use, provide information on the true morphology of defects, damage and fracture. They can also be applied to in-situ observation of the time evolution behaviour of various material science phenomena, such as the formation and growth of defects in various material fabrication processes, and the formation and evolution of damage and fracture during use of materials [8 "Sec. 4.6, In Situ

Observations of Deformation / Fracture Behavior, pp. 260 - pp. 261"]. Furthermore, it provides a new paradigm for understanding the mechanical behaviour of materials through visualisation [8 "Sec. 6.6.6 , Tomography for Polycrystalline Structures, pp. 372 - pp. 373", 15] of polycrystalline microstructures, 4D mapping of chemical composition [8 "Sec. 5.4.1 , Absorption-Edge Subtraction Imaging, pp. 312 - pp. 315", 16] and driving forces for crack propagation [8 "Sec. 9.2.3.1, Local Fracture Resistance Mapping, pp. 513 - pp. 517", 17]. X-ray microtomography has also been applied to creep failure problems in steel and other materials in several cases [6, 18-31]. Many of these involve the preparation of micro specimens of structural materials such as steel and aluminium, and in-situ observation of phenomena such as creep rupture and creep fatigue occurring somewhere between a gauge section [6, 18-28]. On the other hand, new approaches have been reported, such as devising experimental techniques to investigate the effects of very heterogeneous microstructures such as welds [29, 30] and directly measuring three-dimensional stress and strain localisation in the specimen [31]. The former approach is described in detail below. In the latter, creep tests of an Al-Mg alloy at 773 K have been carried out to directly measure the non-uniform creep strain by measuring the physical displacement of tens of thousands of dispersion particles that can be observed between a specimen gauge section. The results have shown that the fracture is dominated by non-uniform hydrogen precipitation on grain boundary particles that had already existed before loading [25].

Ref 29 and 30, which investigated creep rupture behaviour in welds of high-alloy steels, both cut out miniature specimens necessary to obtain the high resolution in X-ray microtomography observation from large specimens or real components for observation. Schlacher et al. prepared creep specimens so that the weld metal, HAZ and base metal were all included between the gauge sections of the specimens and creep tests were carried out in a 9Cr-3W3Co steel with 0.012 % B. One specimen for X-ray microtomography was cut out from the creep specimen after the creep test, and locally significant creep void formation was observed in fine grain regions along the prior austenite grain boundaries [29]. They concluded that, although the overall boron addition suppresses fine grain formation and acts in the direction of preventing creep rupture, the localised fine grains previously present can lead to creep rupture. On the other hand, Tsuruta et al. prepared weld joint specimens similar to those of Schlacher et al. in a 9Cr-1V steel and interrupted the creep test at five levels of creep test time, corresponding to 17.7 - 80 % of the creep lifetime [30]. In this study, specimens for X-ray microtomography were cut along the narrow HAZ bands of the interrupted specimen at nine locations. This allowed the distribution of creep voids in the thickness direction and their time evolution behaviour to be evaluated. The results revealed that creep void growth is accelerated at certain locations in the HAZ, which seems to correspond to high and low stress triaxiality depending on the weld metal and HAZ geometry. The interaction between creep voids causes localised creep void growth and coalescence, and the effectiveness of such 4D observations was demonstrated.

A number of creep models have been proposed to promote physical understanding of creep failure mechanisms and to contribute to design and reliability improvement through engineering creep life prediction [32]. These can be categorised into those based on modelling creep void growth mechanisms, those based on the classical plasticity theory and those based on the continuum damage mechanics. Speight & Harris and Hull & Rimmer's models [33, 34], which are based on the growth and coalescence of creep voids at grain boundaries and is governed by diffusion at grain boundaries, Needleman & Rice and Cocks & Ashby models [35, 36], which couple diffusion and power law creep, Dyson's model [37], which formulates the constraint effect of neighbouring grains. Ogata proposed a void growth model that considers a combined mechanism of diffusion and power law creep deformation under constrained conditions of neighbouring grains [38]. The void growth models under creep conditions that have been proposed can be divided into the "diffusion control model" [33, 34], the "diffusion and power creep deformation control model" [35, 36], and the "diffusion control constraint effect consideration model" [37]. The void growth equations are derived from each model, and void growth observations show that isolated voids mainly occur at grain boundaries inclined from the stress axis and that the cavity shape changes from spherical to crack-like. Based on these observations, it is concluded that cavity growth models should consider growth and cavity shape transitions governed by constraining effects on diffusion and power creep deformation.

A model has been proposed to predict creep rupture life for high Cr steel welded joints where such Type IV failures occurred [39, 40]. These models are validated and modified based on observations of interrupted creep tests at various temperature, stress, and test duration conditions for void initiation, growth, and coalescence. The model cannot be properly validated without continuous observations of increasing void number density and size in a single specimen.

Tsuruta et al. have somehow achieved a 4D observation to provide an overview of Type IV fracture by examining the time evolution behaviour by cutting out tomography specimens from multiple specimens with different elapsed times and the spatial distribution by cutting out multiple specimens from different locations, respectively [30]. However, unless the time evolution behaviour of individual creep voids is clarified, the relationship between the formation, growth and coalescence behaviour of creep voids and the microstructural and mechanical conditions cannot be properly understood.

The aim of the present study was to deepen the findings of Tsuruta et al. by conducting continuous observations of the same specimen, and to identify detailed creep void formation, growth and coalescence processes, the driving forces for creep void growth and their temporal variation, and the engineering parameters that represent type IV damage. High-resolution X-ray microtomography, which can be used to visualise microstructures, was used for this purpose. It is physically difficult to observe the weld metal, HAZ and base metal all within the narrow field of view of a miniature specimen of the order of 1 mm. Therefore, an annular notch was introduced into the miniature creep specimen cut from the HAZ to enhance the stress triaxiality [41] that governs the driving force for creep void growth [42] and creep tests were conducted to simulate a welded joint. As it is not possible to complete the normal creep tests within a few days of ordinary beam time of the synchrotron radiation experiments, all experimental data were obtained by repeating the creep loading in the laboratory and the synchrotron experiments once or twice every six months for in total about three years as ex-situ observations. In Chapter 4, the applicability of the classical void growth model [33-37] and the Ogata model [38] was examined based on the observed data of void shape, spatial distribution, and growth rate with time obtained by 4D observations.

2. Experimental methods

2.1 Specimen

In the present study, the formation, growth and coalescence behaviour of individual creep voids were observed and measured by continuously observing the creep damage and fracture process of the same specimen. For this purpose, a miniature creep specimen was taken from the HAZ fine-grained region of a weld joint as shown in Fig. 1. First, a modified 9Cr-1Mo steel (ASME Grade 91 steel) of 80 mm thickness and 35 mm width was tempered at 1050 ºC for 95 min and then at 780 ºC for 95 min. The details of chemical composition are 8.55Cr-0.98Mo-0.43Mn-0.37Si-0.19V-0.1C-0.08Nb-0.04Ni-0.014P-0.002S in mass%. The mechanical properties of this material at room temperature and 650 °C in the direction of the rolled plate width are 528 and 194 MPa for 0.2 % proof stress, 687 and 271 MPa for tensile strength, 22.7 and 28.7 % for elongation and 74.8 % and 93.7 % for reduction in area, respectively.

After machining a V-shaped groove with a groove angle of 3° and a depth of 80 mm perpendicular to the rolling direction, a weld joint was produced as shown in Fig. 1 by TIG welding and residual coating shielded arc welding. This was further subjected to a post-weld heat treatment at 740 °C for 3.5 h. Fig. 1 also shows details of the miniature creep specimen. In a previous report, the stress triaxiality of the weld joint was evaluated [30]. To simulate this, a V-shaped annular notch with a depth of 0.55 mm at 60° was introduced in the centre of a specimen gauge section. The diameter of the notch bottom is 0.9 mm.

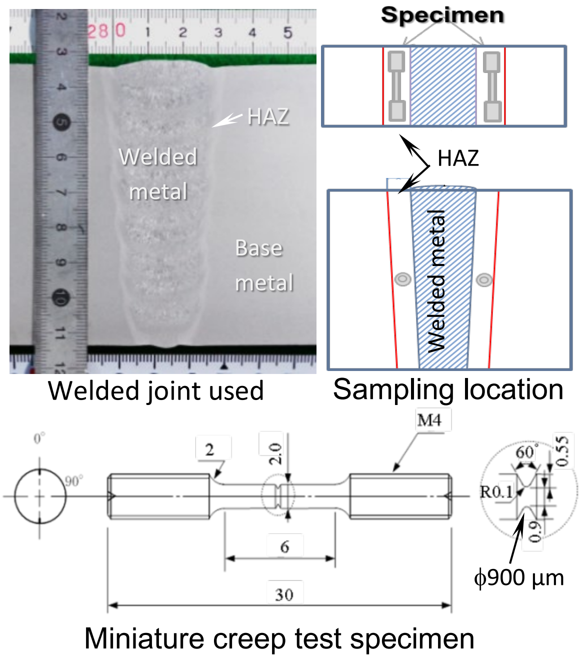

Fig. 1 Miniature creep test specimen and its location for specimen sampling in a welded joint.

2.2 Ex-situ creep tests and X-ray microtomographic observation of creep rupture process

Creep tests were carried out in an inert gas atmosphere at a temperature of 650 °C and a nominal stress of 70 MPa, with an argon gas flow of 99.99 % purity to prevent oxidation. The creep rupture life, t_r, under these conditions was 1633.5 h. The elapsed time, t, divided by the creep rupture life is referred to as the non-dimensional test time, t / t_r. Fig. 2 shows the curve between creep strain and creep test time. The creep strain was calculated from the change in gauge length of the specimen for convenience. As shown in the figure, the creep test was interrupted at the non-dimensional test times t / t_r = 0 % (t = 0 h), 17.8 % (t = 290.0 h), 41.8 % (t = 682.0 h), 62.6 % (t = 1023.0 h), 73.1 % (t = 1194.0 h), 83.6 % (t = 1365.0h), 94.0 % (t = 1536.0 h) and 99.2 % (t =1621.0h), and the interior of the creep specimen was observed 9 times including fractured specimen. The slope of the creep curve was generally constant between t / t_r of 41.8 % and 62.6 %, indicating a steady-state creep regime. On the other hand, after t / t_r = 62.6 %, the creep strain rate accelerates in the accelerated creep regime.

Ex-situ observations of the creep test were carried out by employing the projection X-ray tomography at the beamline BL20XU of the SPring-8 synchrotron radiation facility. The X-ray energy was 37.7 keV and the sample-to-detector distance was 65 mm. 1800 projection images were acquired while the sample was rotated over 180°. The exposure time was 800 msec. The obtained set of projection images was reconstructed into a 3D image using the convolution back-projection method [8 “Sec. 3.3.3, Convolution Back Projection, pp. 87 - pp. 91”]. The voxel size of the 3D images obtained by the X-ray microtomography is 0.5 μm and the substantial spatial resolution is approximately 1μm. High-resolution 3D images were obtained as per the theoretical resolution [8 "Sec. 7.5, Spatial resolution, pp. 400 - pp. 410"] of the method.

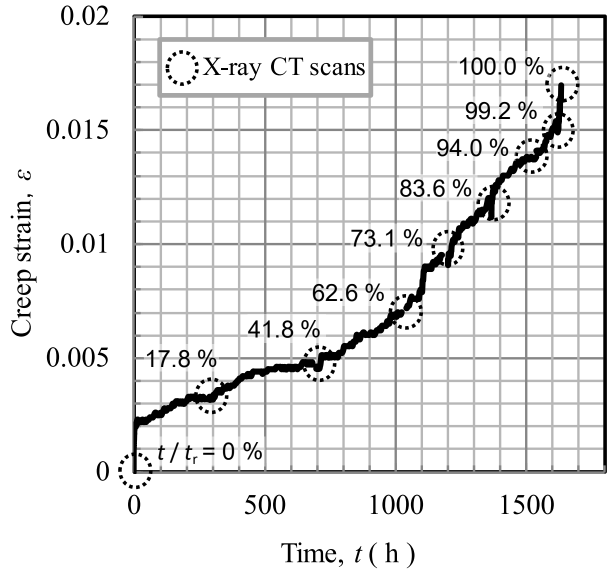

Fig. 2 Creep strain as a function of creep test time and the normalized test times, t / t_r, at which the X-ray microtomography observations were performed.

2.3. Stress analysis by finite element method

To evaluate the stress distribution near the specimen notch, a viscoelastic analysis was carried out using the general-purpose finite element analysis code ABAQUS ver.612. Fig. 3 shows the part of a simulation model. The external shape of the model was the same as the outer morphology of the specimen in Fig. 1. In the area 450 mm from the bottom of the notch, the element size was set to gradually become finer towards the bottom of the notch. The smallest element size at the bottom of the notch is 10 μm. The total length of the model was 6 mm and the areas outside the notch bottom were uniformly meshed with coarse elements of size 20 μm. The element used was an axisymmetric shell element with 3914 nodes and 3800 elements.

The input Young's modulus was 125.4 GPa, which is the value of the material used at 650°C [32] Poisson ratio was set to 0.3. For the creep constitutive equation, the Norton law shown in equation (1) was used.

$$\dot{\varepsilon} = \beta \sigma_e^n \qquad (1)$$

where σ_e is equivalent stress. Creep coefficient, β, and creep index, n, were set to 4.53 x 10^{-15} ($MPa^{-n}h^{-1}$) and 5.97, respectively, which were taken from a previous report on creep tests with heat treated smooth round bar specimens to reproduce HAZ [32].

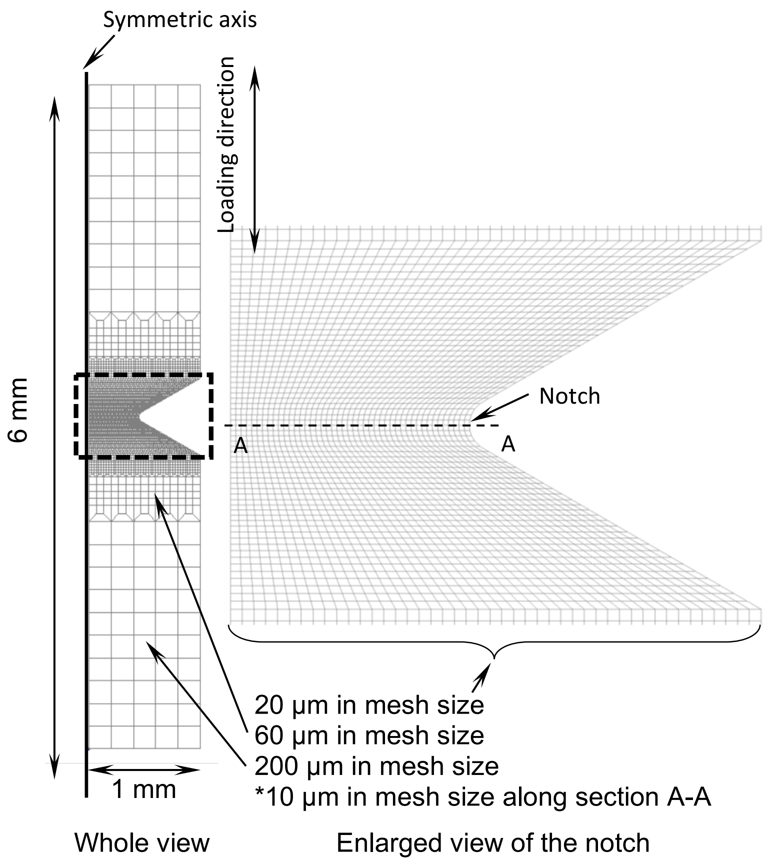

Fig. 3 A model for the elasto - creep finite element analysis. Axisymmetric shell elements were used with the rotation symmetry condition. Stress concentration factor for the notch root was 2.45.

3. Experimental and analytical results

3.1 Finite element method analysis

Fig. 4 shows the results of the finite element analysis. It shows the distribution of the maximum principal stress, σ_1, the hydrostatic stress, σ_m, the von Mises equivalent stress, σ_e, and the stress triaxiality, σ_m / σ_e, along the A-A section in Fig. 3. All the stress components were taken their maximum values on this A-A cross-section; Fig. 4 shows the data at a load of 70 MPa and a test duration of 1633.5 h. σ_1, σ_m, σ_e and σ_m / σ_e have maxima at 50-60, 60-70, 0-10 and 110-120 µm from the bottom of the notch, respectively. The maximum values at the locations were 86 MPa, 59 MPa, 56 MPa and 1.45 respectively. The values of σ_m / σ_e is 0 for simple shear, 0.333 for uniaxial tension and

0.666 for biaxial tension. In the present study, the values are very high compared to these due to sharp notches. Kobayashi et al. found in their elasto-plastic analysis of maraging steel that when the notch bottom radius of the V-shaped annular notch is 0.1 mm, as in the present study, the maximum value of σ_m / σ_e is maximum a little inside the notch bottom, and for higher notch-tip radii the maximum values are at the notch bottom [43]. The maximum value of σ_m / σ_e = 1.53 was shown in their research. As the deformation mode is different (i.e. viscoelastic) in this study, the values of σ_m / σ_e are slightly lower, but otherwise the agreement is generally good. Judging from the obtained stress-strain gradients, the content and conditions of the analysis, such as element size, are judged to be reasonable.

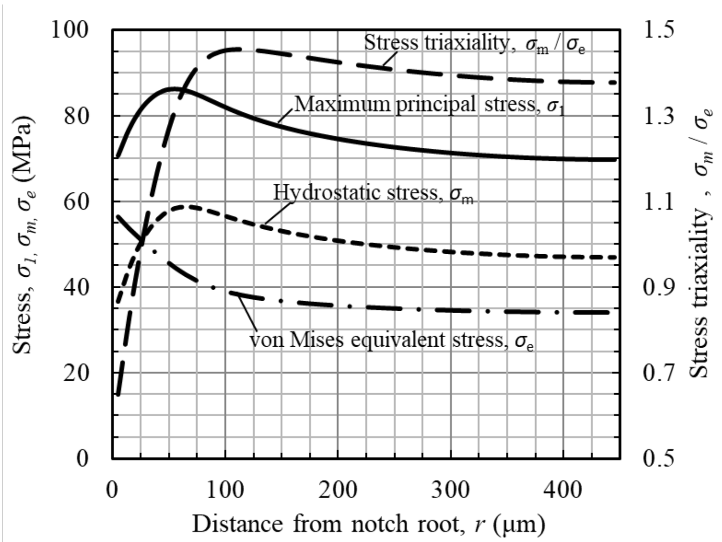

Fig. 4 Results of the finite element analysis, showing the distributions of maximum principal stress, σ_1, hydrostatic stress, σ_m, von Mises equivalent stress, σ_e, and stress triaxiality, σ_m / σ_e as a function of distance from the notch root at t / t_r = 17.8 %.

3.2 3D sequential observation of creep voids

Fig. 5 shows the 3D images of creep voids near the notch in the form of a series of the identical virtual cross-section. Fig. 6 shows the same data in the form of a series of 3D images with limited thickness for easier viewing. In Fig. 5, the particulate feature (A) indicated by the arrow in the image at t / t_r = 0 % is judged to be an inclusion particle based on its linear absorption coefficient. The number and size of creep voids increased with increasing creep test time up to t / t_r = 41.8 %, and their formation at a greater distance from the notch bottom can also were confirmed. At t / t_r = 83.6 %, the creep void coalescence became more pronounced, as new micro-creep voids were formed between coarse creep voids. Subsequently, at t / t_r = 99.2 %, the formation of a main crack due to creep void coalescence near the bottom of the notch was observed: particle A in the image at t / t_r = 0 % in Fig. 5

generates new creep voids at t / t_r = 73.1 % by interfacial debonding, which eventually grew larger and connected with the surrounding creep voids. It can be clearly observed that it directly contributed to the formation of the fracture surface as a main crack at t / t_r = 99.2 % with a length of more than 150 μm (B in the figure).

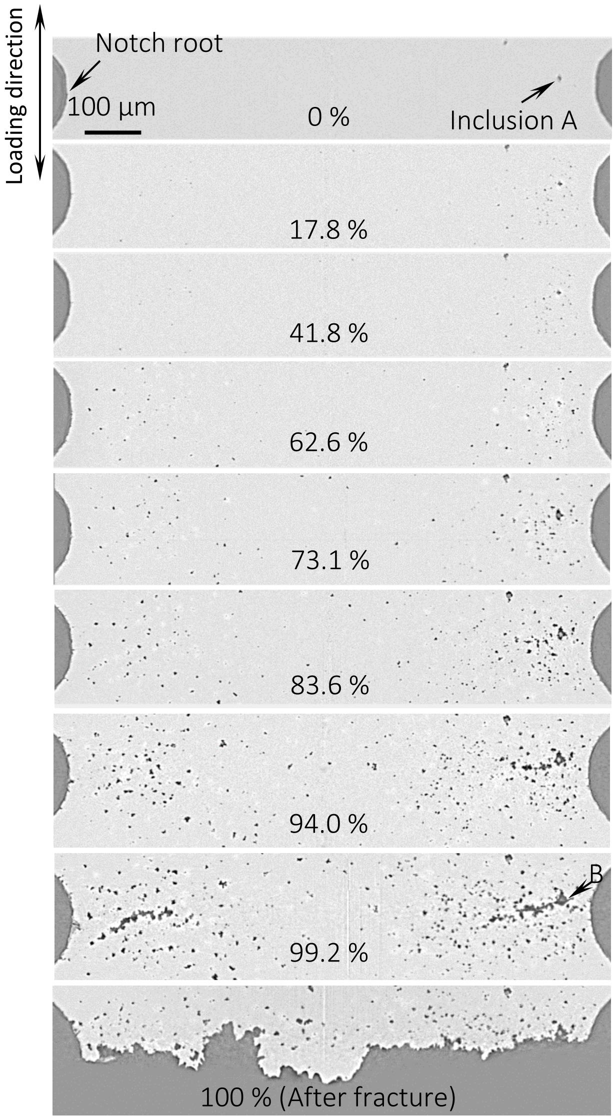

Fig. 5 Void growth behaviour displayed on an identical virtual cross section. The percentage value indicated for each image is the ratio between test time and the total creep lifetime. Void B shown in the 99.2 % image was initiated around inclusion A shown in the 0 % image.

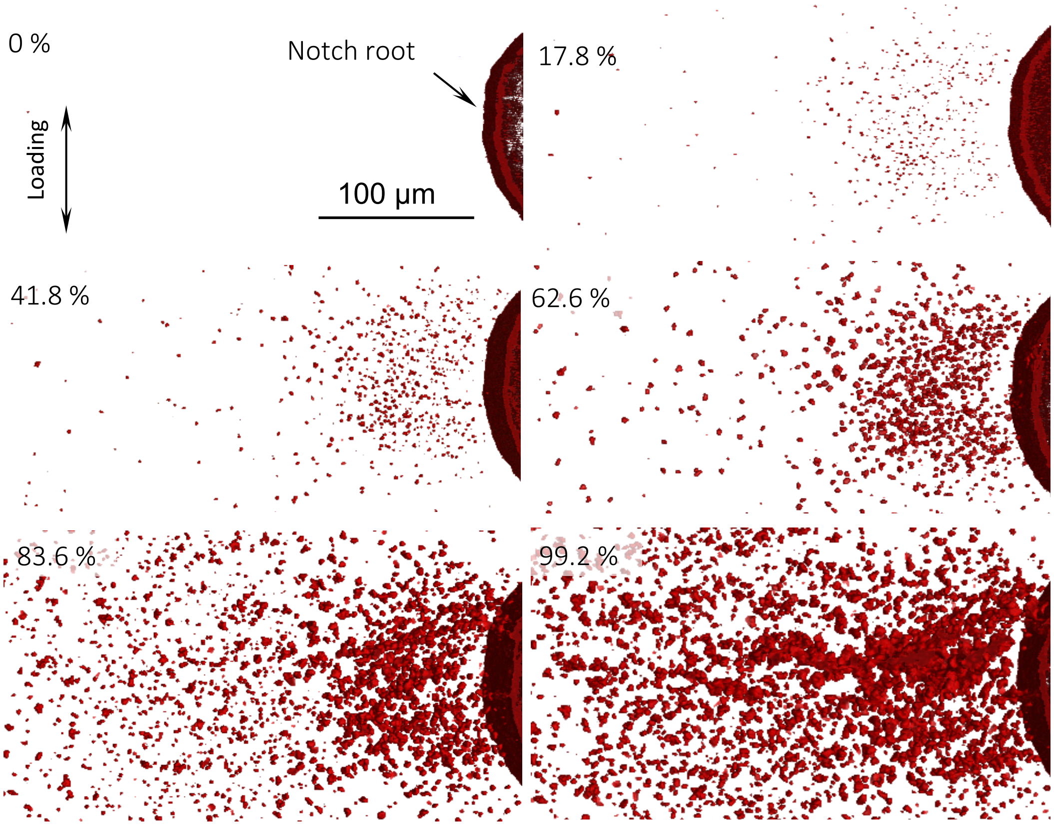

Fig. 6 4D void growth behaviour viewed as a series of 3D images (thickness of each image was limited to 50 μm for visibility) near the notch. The percentage value indicated for each image is the normalized test time. Note that only creep voids are shown in red, and the underlying iron and dispersed particles are not displayed.

Comparing the stress distribution in Fig. 4 with the virtual cross sections shown in Fig. 5, significant creep void formation was observed between the notch bottom and the location about 150 μm from the notch bottom where the maximum principal stress, σ_1, and hydrostatic stress, σ_m, are high. Creep tests on weld joints carried out by the present authors have shown that the volume fraction of creep voids was significantly higher in the region of high maximum principal stress and hydrostatic stress due to the localisation of these stresses caused by differences in the mechanical behaviour of the weld metal, HAZ and base material [30, 32]. By considering the microstructure of FGHAZ in the V-notch specimen and simulating the behaviour of FGHAZ being constrained in the weld metal and parent phase of the welded joint test piece due to the notch effect, it matched the creep failure mode of the welded joints. The 73.1 % and 83.6 % images in Fig. 5 show that significant creep void growth occurred at a distance of about 100 μm from the notch bottom where the stress triaxiality is maximal.

3.3 Quantitative evaluation of creep voids

To quantitatively verify the observations in section 3.2, the number and volume of creep voids were calculated from the X-ray microtomography images. The image analysis method and other details for this are detailed in the literature [8 "Sec. 8.5, Quantitative Geometric Analyses, pp. 476 - pp. 481"]. Here, the regions were delimited every 50 μm from the bottom of the notch and the number density and volume fraction of creep voids in each region were calculated.

First, the void number density, organised by distance from the notch bottom, is shown in Fig. 7(a). In the steady-state creep range of 41.8 to 62.6 % in t / t_r, the number density of creep voids was maximum in the range 50 to 100 μm from the notch bottom. This is also consistent with the positions where the hydrostatic stress and maximum principal stresses are elevated. On the other hand, in the accelerated creep region, after t / t_r = 62.6 %, coalescence of creep voids occurs, as revealed by the above observations. In the region from 50 to 100 μm from the bottom of the notch, the number density decreased with the coalescence of the creep voids and the maximum number density value moved towards the centre of the specimen. On the other hand, the creep void volume fraction shown in Fig. 7(b) continued to increase after the coalescence of the creep voids and the position of the maximum void volume fraction did not change. The authors conducted substantive creep tests on weld joints to investigate the 3D morphology and spatial distribution of creep voids in Type IV damage in the HAZ fine-grained region [30] and showed that the void volume fraction is an effective parameter for evaluating the degree of the progress of Type IV damage. This is consistent with the results of the present miniature creep tests.

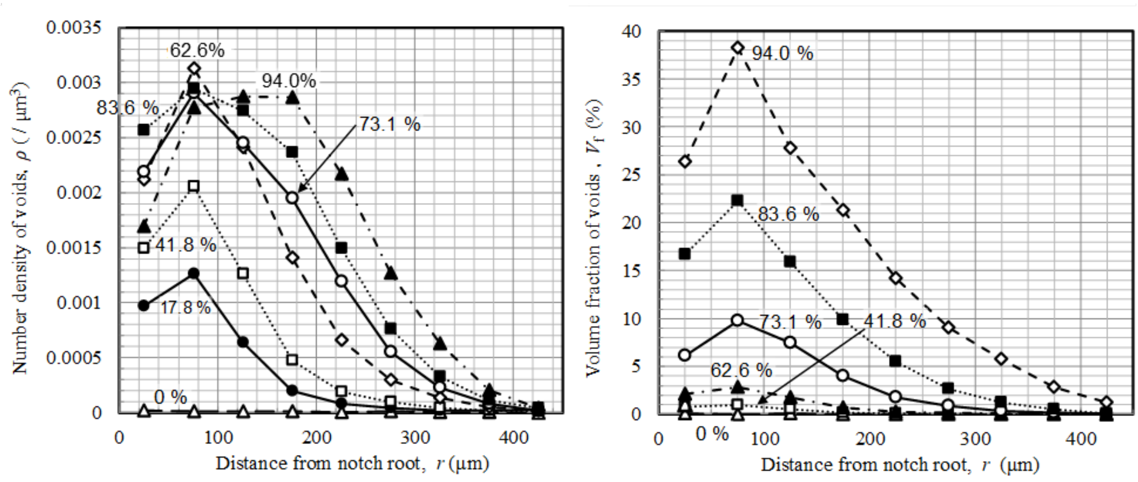

(a) Void number density (b) Void volume fraction

Fig. 7 The distributions in number density and volume fraction of creep voids as a function of distance from a notch bottom, which are separated by the normalized test time at which the creep voids are formed.

4. Model analyses and their validation for creep void formation and growth

4.1 Creep void formation

Fig. 8 shows the change in number density in the regions of 100 to 150 μm, 150 to 200 μm, 200 to 250 μm and 250 to 300 μm in distance from the bottom of the notch.

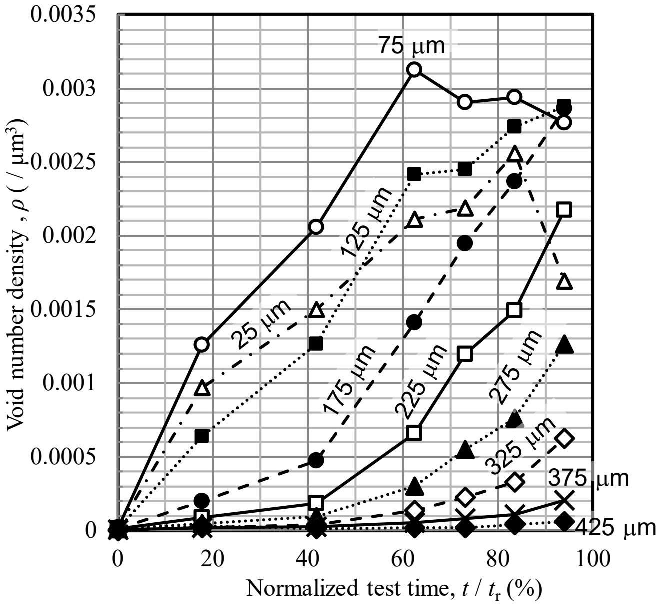

Fig. 8 Experimental void initiation behaviour expressed as void number density as a function of normalized test time for different distance from the notch root.

Next, Fig. 9 shows the creep void growth curves generated at each loading stage. Here, the position, volume and shape in the 3D image were first measured precisely for all creep voids found in the final loading step. The identical creep voids in the 3D images were then identified and traced backward in time from the final loading step towards the initial unloaded step. In this way, the loading steps at which individual creep voids were formed were identified and creep void growth during loading was measured. In Fig. 9, there is no difference in the growth behaviour of creep voids formed at any of the loading steps. It can therefore be seen that the evaluation and control of creep voids formed in the early stages is important, as they eventually grow to larger size. Creep voids formed at any loading stage grow slowly immediately after their formation. Thereafter, steady growth was observed, followed by accelerated growth in the final loading step. The slow growth immediately after formation may be due to the fact that the particles that initiated the creep voids still have constraint effect on the viscoelastic flow of the matrix. On the other hand, the accelerated growth in the final loading step is probably due to the further increase in stress triaxiality due to crack initiation.

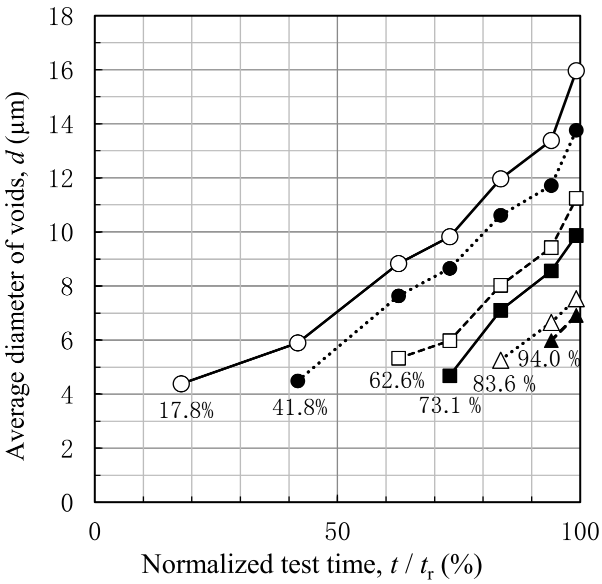

Fig. 9 Comparison in experimental void growth curves for voids initiated at 6 different test times. Those for the voids nucleated at 125 μm are shown.

Next, out of the data in Fig. 9, only the creep voids that formed early (in t / t_r = 17.8 %) were extracted and organised according to the distance from the bottom of the notch at the location of formation, as shown in Fig. 10. Note that the data for r = 400 - 450 μm are unreliable due to the small number of data points. Creep voids grow significantly in the region of r = 50 - 200 μm from the bottom of the notch, where the maximum principal stress, hydrostatic stress and stress triaxiality are maximum. However, in the steady creep regime, the difference is not so great. In the accelerated creep regime, on the other hand, the creep void growth is particularly large in the r = 50 - 200 μm region. This indicates that the influence of the individual stress components on individual creep void growth is not very significant, and that creep void coalescence has a strong influence on creep void growth in the accelerated creep regime. Therefore, when looking at creep void growth in type IV damage, the coalescence between creep voids should be taken into account.

Fig. 11 shows the size distribution of creep voids (t / t_r = 17.8%) initiated early at a distance r = 125μm from the notch root. The void size distribution at each normalized test time is shown for the void contained at r = 125μm in Fig. 10. The peak position of the relative frequencies shifts to the right as the normalized test time increases were confirmed. It was also observed that the growth rate of individual voids differs within a distance r = 125 from the notch root. Since void growth is affected by grain size and the presence of inclusions on the grain boundary, it is assumed that a comparison with the local stress state at the grain boundary is necessary to evaluate the variation of these void growth rates. Creep void size distributions for all ranges except r = 125μm from the bottom of the notch are shown in Appendix A.

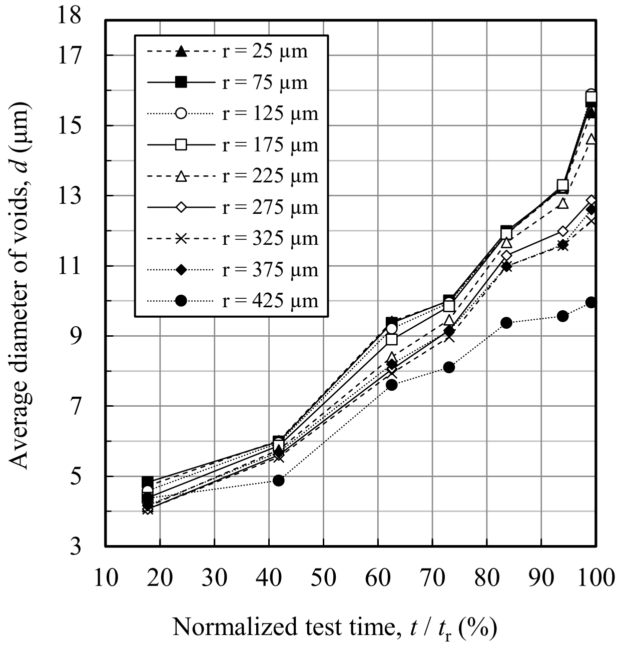

Fig. 10 Experimental void growth curves for voids initiated at different levels in the distance from the notch root.

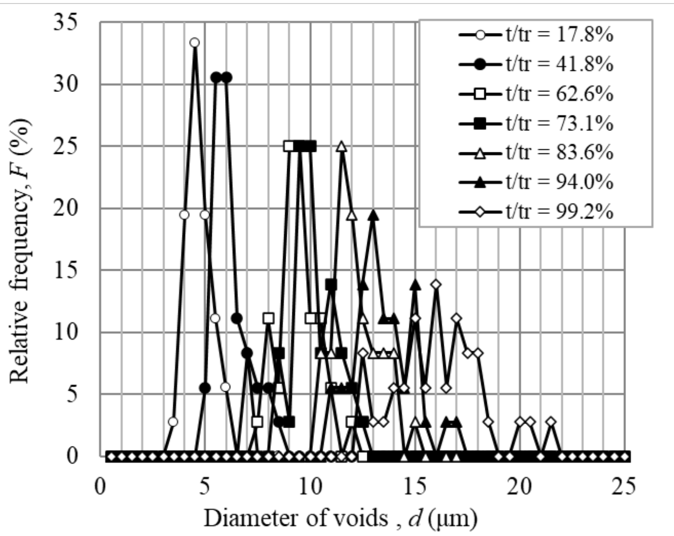

Fig. 11 The distributions in size of creep voids at distance r = 125μm from a notch bottom, which voids initiated at the normalized test time t / t_r = 17.8%.

4.2 Creep void growth

A number of creep models have been proposed to promote physical understanding of creep failure mechanisms and to contribute to design and reliability improvement through engineering creep life prediction [32]. These can be categorised into those based on modelling creep void growth mechanisms, those based on the classical plasticity theory and those based on the continuum damage mechanics. Of these, the present study attempted to understand the phenomenon by applying the classical creep void growth models based on the creep void growth mechanisms. The models used were Speight & Harris and Hull & Rimmer's models [33, 34], which are based on the growth and coalescence of creep voids at grain boundaries and is governed by diffusion at grain boundaries, Needleman & Rice and Cocks & Ashby models [35, 36], which couple diffusion and power law creep, Dyson's model [37], which formulates the constraint effect of neighbouring grains, and Ogata's model, which adds the constraint effect of neighbouring grains to the coupling of diffusion and power creep law [38].

The experimental data and the prediction of each model are plotted in Fig. 12. Here, the data for creep voids formed as early as t / t_r = 17.8 % at distances r = 100 to 150 μm from the notch bottom are shown. Focusing on the region up to t / t_r = 83.6 %, where no significant creep void coalescence occurs, it can be seen that the Ogata model, which takes into account the constraining effect of neighbouring grains, is relatively close to the experimental data. The growth curve of creep voids formed at each loading stage and the corresponding prediction of the Ogata model are shown in Fig. 13, also for data at distances r = 100 to 150 μm from the bottom of the notch. The creep void growth model and respective parameters of Ogata et al [38]. are shown in Appendix B. Only for the early creep voids (t / t_r = 17.8 %), there is a good agreement between the model and the experimental measurements. However, for creep voids formed later, there are significant differences between the experiment and the model. In particular, the later the creep voids occur, the larger the difference. This may be due to the fact that creep voids formed later in the loading steps have relatively large creep voids in their vicinity and the accelerated growth due to their influence cannot be taken into account. Therefore, the differences between experimental and model predictions are wider for those formed later and for the more advanced loading steps.

Fig. 9 shows that there is no difference in the growth behaviour of creep voids generated at either loading stage, indicating that it is important to assess and control creep voids generated at earlier stages. This is also evident from the experimental observations in Fig. 5 and Fig. 6. Therefore, the use of Ogata model is expected to be effective for such purposes.

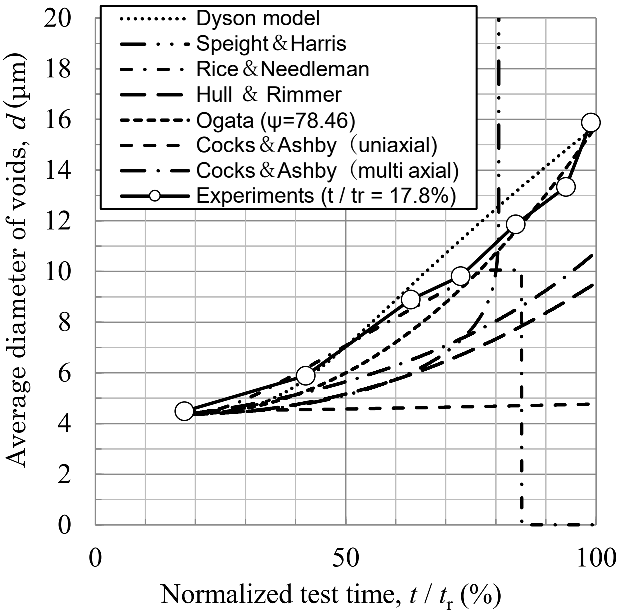

Fig. 12 Comparison of void growth models together with the experimental void growth curve for voids initiated at 125 μm from the notch root.

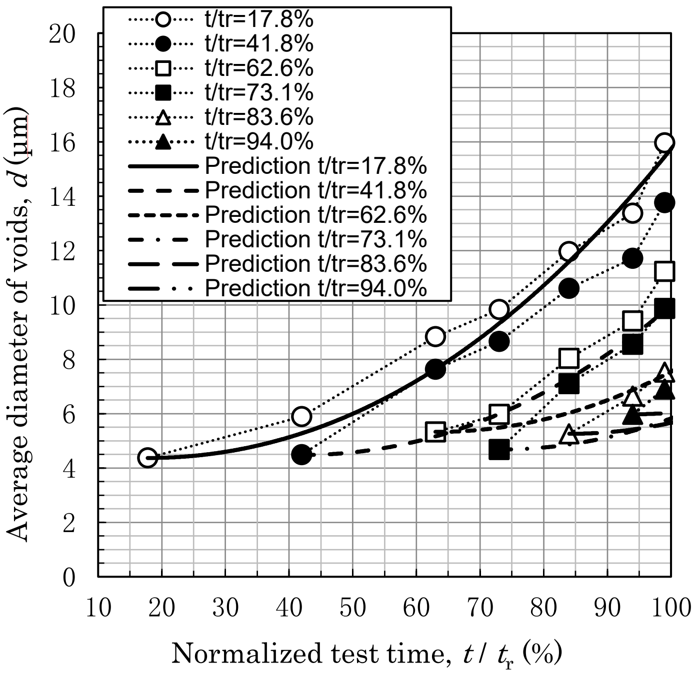

Fig. 13 Comparison of Ogata model and the experimental void growth curve for voids initiated at 125 μm from the notch root.

5. Conclusion

To investigate the effect of stress state on creep void formation and growth in the HAZ fine-grained region of a modified 9Cr-1Mo steel, the creep damage process in one specimen was continuously observed in three dimensions using the X-ray microtomography technique. The formation, growth and coalescence behaviour of individual creep voids over time was measured and analysed, and quantitatively measured in the form of changes in the size of individual creep voids. This was combined with the finite element analysis simulating the specimen to calculate the stress distribution in the vicinity of the notch to clarify the effects of the stress state.

The maximum principal and hydrostatic stresses are greatest a little further inwards from the bottom of the notch. The growth and coalescence of creep voids were promoted on the grain boundaries in the region where the maximum principal stress and hydrostatic stress are high. Creep voids that are formed early eventually grow to a larger size, so their assessment and control is important. Their growth and coalescence with the surrounding creep voids results in the formation of a main crack, which directly contributes to the formation of the fracture surfaces. The location of the stress triaxiality maximum is slightly closer to the centre of the specimen than the location of the maximum principal or hydrostatic stresses, where creep void growth is more pronounced. These are consistent with the test results for welded joints in the literature. In the steady-state creep region (t / tr = 41.8 ~ 62.6%), the influence of stress parameters such as σ_1, σ_m, σ_m/σ_e is not significant, and the creep void coalescence has a strong influence on creep void growth in the accelerated creep regime.

The growth of creep voids that are formed early in the loading step can be well approximated by the Ogata model, which combines diffusion and power-creep law coupling with the constraint effects of neighbouring grains. For creep void growth occurring at later loading steps, the Ogata model underestimates it. Other engineering evaluation parameters for the progress of type IV damage were also investigated.

Acknowledgements

HT is grateful to support by JSPS KAKENHI Grant Number JP21H04624. The synchrotron experiments were performed with the approval of JASRI, through proposal numbers 2015A1712, 2015B1617, 2016A1539, 2017A1547 and 2017B1586.

Appendix A

Creep void size distributions for all ranges except r = 125μm from the bottom of the notch were shown in Figure A1. The horizontal axis indicates void size, and the vertical axis indicates relative frequency. As the normalized test time increases, the peak position of the relative frequency shifted to the right. As seen in Figure 10, coarse voids are largely contained at distances r = 50-200 from the bottom of the notch. In order to evaluate such differences in the amount of void growth, it is important to calculate the local stress acting on the grain boundary by incorporating the grain size, grain boundary angle, etc. into the FEM model and evaluate the relationship between this local stress and the amount of void growth.

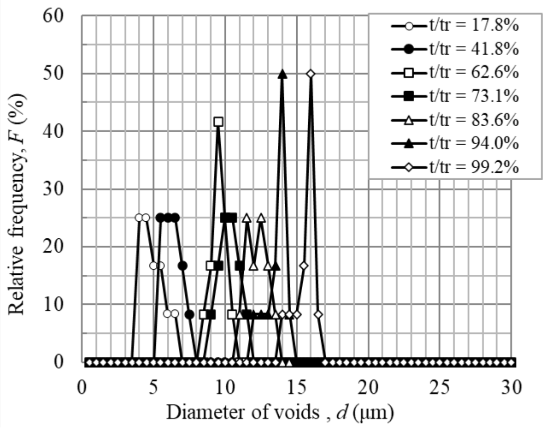

(a) r = 25 μm

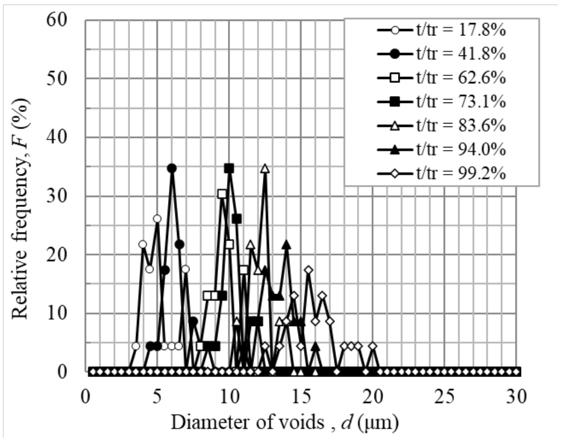

(b) r = 75 μm

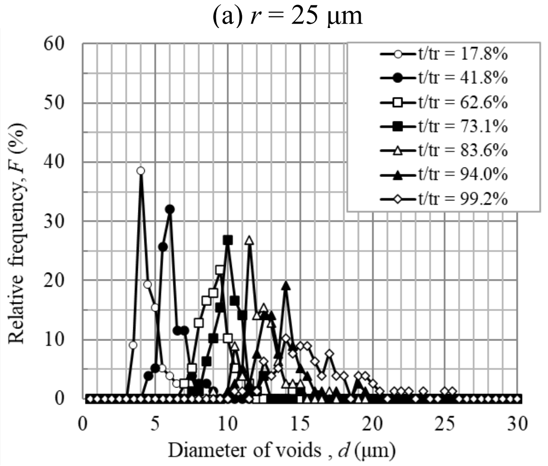

(c) r = 175 μm

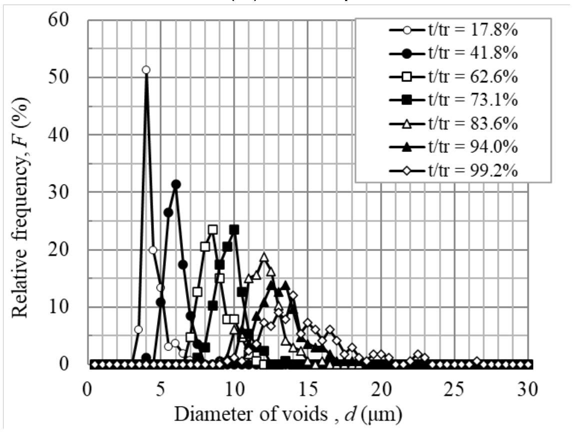

(d) r = 225 μm

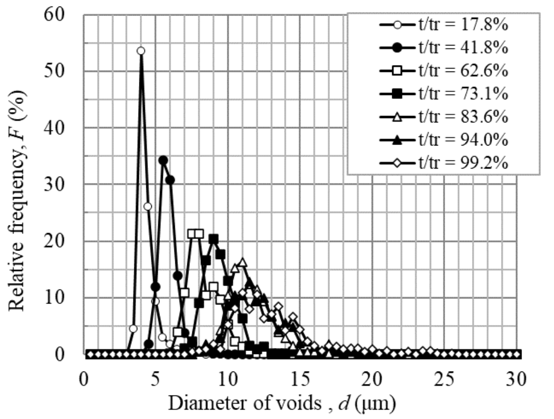

(e) r = 275 μm

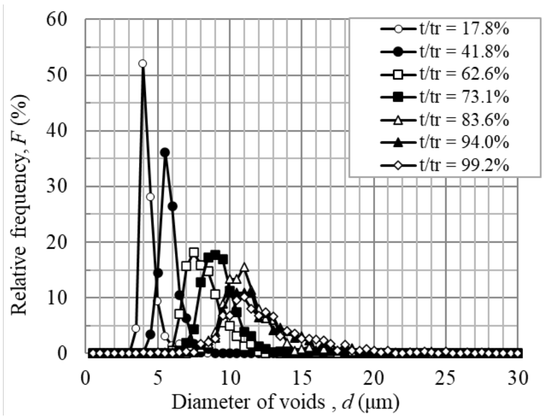

(e) r = 325 μm

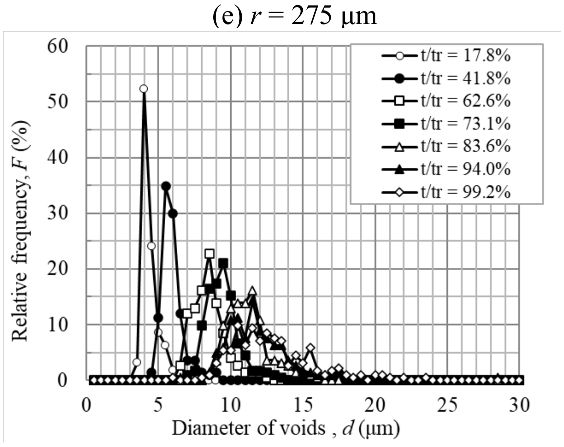

(f) r = 375 μm

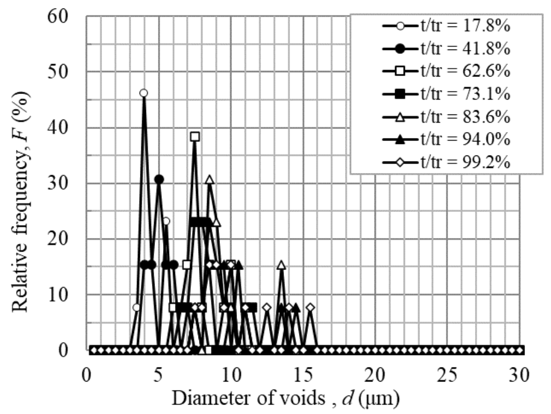

(g) r = 425 μm

Fig. A1 The distributions in size of creep voids at distance r = 25, 75, 175, 225, 275, 325, 375, 425μm from the notch root, which voids initiated at the normalized test time t / tr = 17.8%.

Appendix B

Ogata et al. proposed the void growth model considering combined mechanism of diffusion and power law creep deformation under constrained condition for the void growth and derived the void growth rate equations for spherical and crack-like voids [38]. The void growth equations for the spherical and the crack-like voids are expressed by the following equations.

(Spherical void)

$$\frac{d_a}{d_t} = \frac{a\dot{\varepsilon}_c}{2h(\psi)}(\frac{\Lambda}{a})^3[L+M]^{-1} \quad \text{(B1)}$$

(Crack-like void)

$$\frac{d_a}{d_t} = \frac{\alpha a\dot{\varepsilon}_c}{4\pi h(\psi)}(\frac{\Lambda}{a})^{\frac{5}{2}}[L+M]^{-\frac{3}{2}} \quad \text{(B2)}$$

$$\Lambda = (\frac{\delta_b D_b \Omega \sigma_n}{kT\dot{\varepsilon}_c})^{\frac{1}{3}} \quad \text{(B3)}$$

$$h(\psi) = \left[\frac{1}{1+cos\,\psi - \cos(\psi)/2}\right]/sin\,\psi \quad \text{(B4)}$$

$$L = \frac{2b}{\beta d}(\frac{\Lambda}{a+\Lambda})^3 \quad \text{(B5)}$$

$$M = \ln[\frac{a+\Lambda}{a} - \left[3-\left[\frac{a}{a+\Lambda}\right]^2\right]\left[1-\left[\frac{a}{a+\Lambda}\right]^2\right]/4] \quad \text{(B6)}$$

$$\alpha = \left[\frac{4\pi h(\psi)}{\left(4\sin\left(\frac{\psi}{2}\right)\right)^{\frac{3}{2}}}\right][(\frac{\delta_b D_b}{\delta_s D_s})(\frac{\sigma_n \Lambda}{\gamma_s})]^{\frac{1}{2}} \quad \text{(B7)}$$

where a is a void radius (m), ψ is a void tip angle (deg.), $\dot{\varepsilon}_c$ is creep strain rate (s^{-1}), δ_b is grain boundary width (m), D_b is grain boundary diffusion coefficient (m^2/s), Ω is atomic volume (m^3), k is a Boltzmann constant (J/K), T is absolute temperature (K), b is void space (m), d is grain diameter (m), δ_s is diffusional thickness of the surface (m), D_s is surface diffusion coefficient (m^2/s), γ_s is surface tension force (J/m^2) and β is a material constant. Based on the in-situ observation of the specimen during creep deformation by X-ray microtomography shown in Fig. 6, the average diameter of the creep voids was predicted by Equation (B1) because the voids are spherical shape until they coalesce to form cracks. The parameters used to predict the void diameters are listed in Table B1.

Table B1 Physical properties used in the simulation.

	ψ (deg.)	β	$\delta_b \cdot D_b$ (m^3/s)	Ω (m^3)	k (J/K)
Value	78.46	0.9	1.00×10^{-22}	1.21×10^{-29}	1.38×10^{-23}
Reference	[44]	[44]	[44]	[45]	[45]

References

[1] M. Taneike, F. Abe and K. Sawada: Creep strengthening of steels at high temperatures using nano-sized carbo-nitride dispersions, Nature, 424(2003), 294–296.

[2] F. Abe, S. Nakazawa, H. Araki and T. Noda: The role of microstructural instability on creep behavior of low radio-activation martensitic 9Cr-2W steel, Metall. Trans. A, 23A(1992), 469–477.

[3] G. Eggeler: The effect of long-term creep on particle coarsening in tempered martensite ferritic steels, Acta Metall., 37(1989), 3225-3234.

[4] M.E. Kassner, T.A. Hayes, Creep cavitation in metals, International Journal of Plasticity 19(2003), 1715–174.

[5] V. Tvergaard: Effect of microstructure degradation on creep crack growth, International Journal of Fracture, 42(1990), 145-155.

[6] C. Gupta, H. Toda, C. Schlacher, Y. Adachi, P. Mayr, C. Sommitsch, K. Uesugi, Y. Suzuki, A. Takeuchi, M. Kobayashi, Study of creep cavitation behavior in tempered martensitic steel, Materials Science & Engineering A 564 (2013) 525–538.

[7] G. Dalen, M. Koster: 2D & 3D particle size analysis of micro-CT images, In Proceedings of the Bruker micro-CT User Meeting, Brussels, Belgium, (2012), pp. 3-5.

[8] H. Toda: X-Ray CT, Hardware and Software Techniques, Springer Nature Singapore, Singapore, (2021).

[9] D.J. Abson and J.S. Rothwell, Review of type IV cracking of weldments in 9–12%Cr creep strength enhanced ferritic steels, International Materials Review, 58(2013), 437-473

[10] P. Mayr & H. Cerjak: The impact of welding on the creep properties of advanced 9–12% Cr steels, Transactions of the Indian Institute of Metals, 63(2010), 131–136.

[11] J.A. Francis, W. Mazur and H.K.D.H. Bhadeshia: Type IV cracking in ferritic power plant steels, Materials Science and Technology, 22(2006), 1387–1395.

[12] A. Strang and V. Vodarek: Mater. Sci. Technol., 12(1996), 552–556.

[13] P. Hofer, H. Cerjak and P. Warbichler: Quantification of precipitates in a 10%Cr steel using TEM and EFTEM, Materials Science and Technology, 16 (2013), 1221-1225.

[14] H. Cerjak and P. Mayr: Creep strength of welded joints of ferritic steels, in 'Creep resistant steels', (ed. F. Abeet al.), 472–503;2008, Great Abington, Abington Publishing

[15] H. Toda, Y. Ohkawa, T. Kamiko, T. Naganuma, K. Uesugi, A. Takeuchi, Y. Suzuki, M. Kobayashi: Grain boundary tracking: A four-dimensional visualization technique for determining grain boundary geometry via local strain mapping, Acta Mater. 61(2013), 5535-5548.

[16] H. Toda, K. Shimizu, K. Uesugi, Y. Suzuki, M. Kobayashi: application of dual-energy k-edge subtraction imaging to assessment of heat treatments in al-cu alloys, Mater. Trans, 51(2010), 2045-2048.

[17] K. Shimizu, H. Toda, K. Uesugi, and A. Takeuchi: Local deformation and fracture behavior of high-strength aluminum alloys under hydrogen influence. Metall. Mater. Trans. A 51(2020), 1–19.
[18] X. Zhang, C.P. Cartera, Y. Satapathya, A. Tekawade, J.-S. Parkc, P. Keneseic and M. Li: Understanding creep behaviors of additively manufactured 316L stainless steel via void characterization, Mater. Res. Lett., 11(2023), 806–813.
[19] Z. Tang, H. Jing, L. Xu, L. Zhao, Y. Han, H. Li, N. Ma: Investigation of creep-fatigue crack growth of G115 steel using a novel damage model, Int. J. Mech. Sci., 183(2020), 105827.
[20] H. Fang, N. Szymanski, C.D. Versteylen, P. Cloetens, C. Kwakernaak, W.G. Sloof, F.D. Tichelaar, S. Balachandran, M. Herbig, E. Brück, S. van der Zwaag, N.H. van Dijk: Self healing of creep damage in iron-based alloys by supersaturated tungsten, Acta Mater., 166(2019), 531-542.
[21] L.-Y. Wang, Z.-M. Song, X.-M. Luo, G.-P. Zhang: 3D X-ray tomography characterization of creep cavities in small-punch tested 316 stainless steels, Mater. Sci. Engng. A, 724(2018), 69-74.
[22] T.J.A. Slater, R.S. Bradley, G. Bertali, R. Geurts, S.M. Northover, M.G. Burke, S.J. Haigh, T.L. Burnett and P.J. Withers, Multiscale correlative tomography: an investigation of creep cavitation in 316 stainless steel, Sci. Rep., 7(2017), 7332.
[23] H. Fang, C.D. Versteylen, S. Zhang, Y. Yang, P. Cloetens, D.N.-Tillard, E. Brück, S. van der Zwaag, N.H. van Dijk: Autonomous filling of creep cavities in Fe-Au alloys studied by synchrotron X-ray nano-tomography, Acta Mater., 121(2016), 352-364.
[24] T.L. Burnett, R. Geurts, H. Jazaeri, S.M. Northover, S.A. McDonald, S.J. Haigh, P.J. Bouchard and P.J. Withers: Multiscale 3D analysis of creep cavities in AISI type 316 stainless steel, Mater. Sci. Tech., 31(2015), 522-534.
[25] L. Renversade, H. Ruoff , K. Maile , F. Sket and A. Borbély, Microtomographic assessment of damage in P91 and E911 steels after long-term creep, Int. J. Mater. Res., 105(2014), 621-627.
[26] F. Sket, K. Dzieciol, A. Borbély, A.R. Kaysser-Pyzalla, K. Maile, R. Scheck, Microtomographic investigation of damage in E911 steel after long term creep, Mater. Sci. Engng. A, 528(2010), 103-111.
[27] K.-S. Cheong, K.J. Stevens, Y. Suzuki, K. Uesugi, A. Takeuchi, The effects of microstructure on creep behaviour—A study through synchrotron X-ray tomography, Mater. Sci. Engng. A, 513-514(2009), 222-227.
[28] Y. Shi, B. Du, P. Tang, N. Jin, J. Chen: Study on creep cavity morphology of P91 power plant steel by industrial computed tomography, Proc. SPIE 12626, International Conference on Signal Processing, Computer Networks, and Communications (SPCNC 2022), (2023)126261T.
[29] C. Schlacher, T. Pelzmann ,C. Be´al1, C. Sommitsch, C. Gupta, H. Toda and P. Mayr: Investigation of creep damage in advanced martensitic chromium steel weldments using synchrotron X-ray micro-tomography and EBSD, Mater. Sci. Tech., 31(2015), 516-521.

[30] H. Tsuruta, H. Toda, M. Yatomi, K. Yoshida, A. Takeuchi, M. Uesugi, M. Tabuchi and H. Hongou, Quantitative evaluation of creep voids in mod.9Cr-1Mo steel welded joints with X - ray micro-tomography, J. of Soc. Mater. Sci, Jap., 68(2019), 599-606.

[31] H. Toda, Z.A.B. Shamsudin, K. Shimizu, K. Uesugi, A. Takeuchi, Y. Suzuki, M. Nakazawa, Y. Aoki, M. Kobayashi: Cavitation during high-temperature deformation in Al–Mg alloys, Acta Mater., 61(2013), 2403-2413.

[32] K. Yoshida, H. Tsuruta, M. Tabuchi, K.-I. Kobayashi: Creep damage evaluation method for welded joints of grade 91 steels, J. Parker, J. Shingledecker, J. Siefert (Eds.), Advances in Materials Technology for Fossil Power Plants, ASM Intern., Materials Park, OH (2016), pp. 544-555.

[33] M.V. Speight, J.E. Harris: The kinetics of stress-induced growth of grain-boundary voids, Metal Science Journal, 1 (1967), pp. 83-85

[34] D. Hull, D. E. Rimmer: The growth of grain boundary voids under stress, Phil. Mag., 4 (1959), pp. 673-687.

[35] C.F. Cocks and M.F. Ashby: On creep fracture by void growth, Progress in Materials Science, 27(1982), 189-244.

[36] Rice, J.R," Constraints on the diffusive cavitation of isolated grain boundary facets in creeping polycrystals Acta Metall. 29 (4), (1981), 675 681.

[37] B.F. Dyson: Constraints on diffusional cavity growth rates, Metal Sci. 10 (10), (1976), pp. 349-353

[38] T. Ogata, T. Sakai and M. Yaguchi: Damage assessment method of P91 steel welded tube under internal pressure creep based on void growth simulation, Int. J. Pressure Vessels and Piping, 87(2010), 611-616.

[39] Q. Xu, Z. Lu and X. Wang: Damage modelling: the current state and the latest progress on the development of creep damage constitutive equations for high Cr steels, Materials at High Temperatures, 34 (3), (2017), pp. 229-237.

[40] Q. Xu, X. Yang, Z. Lu: On the development of creep damage constitutive equations: a modified hyperbolic sine law for minimum creep strain rate and stress and creep fracture criteria based on cavity area fraction along grain boundaries, Materials at High Temperatures, 34 (56), (2017), 323-332

[41] T. Ogata, T. Sakai and M. Yaguchi, Damage characterization of a P91 steel weldment under uniaxial and multiaxial creep, Mater. Sci. Eng. A, 510-511(2009), 238-243.

[42] K. Hatanaka, A.N. Yahya, I. Nonaka and H. Umaki, Initiation of high temperature creep voids in notched components", Jap. Soc. Mech. Engineers, 64(1998), 925-932.

[43] M. Kobayashi, S. Yazawa, T. Takeuchi and H. Toguri: Tensile fracture of 18Ni maraging steel having V-type circumferential notch, J. Jap. Soc. Mater. Sci., 33(1984), 1257-1263.

[44] T. Ogata, T. Sakai and M. Yaguchi, Uniaxial creep rupture property of mod.9Cr-1Mo steel weld joint and proposal of creep damage evaluation method, J. of Soc. Mater. Sci, Jap., 58(2009), 94-100.

[45] T. Ogata and M. Yaguchi, Damage mechanism in weldment of 2.25Cr–1Mo steel under creep–fatigue loading, Engineering Fracture Mechanics, 74 (2007), 945-955.